Photo-Catalytic Activity Improvement for Organic Pollutant Removal in Wastewater using Zinc Oxide Quantum Dots: An Experimental and Modeling Study

Tarek M. Awwad
Department of Civil Engineering, Engineering College, Northern Border University, Saudi Arabia | Department of Civil Engineering, Engineering College, Al-Azhar University, Egypt
tarek.awwad@nbu.edu.sa (corresponding author)

Shaaban M. Shaaban
Department of Electrical Engineering, Engineering College, Northern Border University, Saudi Arabia | Department of Engineering Basic Science, Engineering College, Menofia University, Egypt
shabaan27@gmail.com

Ehab M. Ragab
Department of Civil Engineering, Engineering College, Northern Border University, Saudi Arabia
ehabhosny_3@hotmail.com

Ahmed Mir
Department of Chemical and Materials Engineering, Engineering College, Northern Border University, Saudi Arabia | Research Laboratory Process Engineering and Industrial Systems, National School of Engineers of Gabes, University of Gabes, Tunisia
ahmedmirch@gmail.com

Received: 27 September 2023 | Revised: 8 October 2023 | Accepted: 10 October 2023

 DOI: https://doi.org/10.48084/etasr.6451

ABSTRACT

Photo-catalyst nanoparticles (NPs) find applications in many diverse fields, including environmental remediation, energy conversion, and organic synthesis. By optimizing the nanoparticle's composition, size, morphology, and surface properties, the photo-catalytic performance can be enhanced to develop more efficient and sustainable catalytic systems. This work aligns with this innovative approach and aims to improve the photo-catalytic degradation of Sulfamethoxazole (SMX) through the intensification of the photo-catalyst and the micro-reactor. ZnO-NPs were synthesized using the sol-gel method. Zinc Acetate (Z.A) and sodium hydroxide were used as precursor materials. The resulting ZnO-NPs were characterized for their structure and crystallinity using X-Ray Diffraction (XRD) and the photo-catalytic activity was assessed with a micro-structured polymer reactor. The degradation of SMX through photo-catalysis proceeds through several stages that involve coupled processes, such as the transportation of molecules and chemical reactions. To solve the mathematical equations governing the transport and photocatalytic reaction, COMSOL Multiphysics software was utilized. The characterization results demonstrate the excellent crystallinity and high purity of the synthesized ZnO-NPs, enabling the estimation of the average diameter of the NPs under different synthesis conditions. The grain growth is faster (3.5 hr) at higher temperatures (70, 80, and 90 °C), and slower (4 hr) at lower temperatures (50 and 60°C). The photo-catalytic degradation is significantly more efficient on 16 nm ZnO-NPs than 50 nm ZnO-NPs. At this size, the conversion rate reaches 96%, surpassing the performance of commercial ZnO-NPs, which only degrades 81% of SMX. The conversion rate obtained through simulation is slightly higher than that achieved in the experiments. However, this difference remains negligible, and overall, the model fits well with the experimental data. This validation of the chosen model confirms its reliability and accuracy.

Keywords-ZnO nanoparticles; sulfamethoxazole (SMX); sol-gel method; characterization; microreactor; modeling; simulation

I. INTRODUCTION

Water pollution exacerbates the degradation of natural water quality by modifying its physical, chemical, biological, or bacteriological characteristics [1-3]. To mitigate the rapid escalation of pollution, stringent regulations are in place to govern water designated for human consumption, and these regulations adapt in tandem with technological advancements in analysis methodologies [4, 5]. Among the most dangerous pollutants that significantly impact water quality are antibiotics. Antibiotics are mainly used in the prevention and treatment of human and in the prevention and control of agricultural and aquaculture diseases [6, 7]. Authors in [8] analyzed the trends and drivers of antibiotic consumption from 2000 to 2015 in 76 countries and projected the total global antibiotic consumption until 2030. The study indicated that global antibiotic consumption increased by 65% between 2000 and 2015. Various antibiotics have been reported in different environmental compartments, such as wastewater from treatment plants, river waters, sediments, and soils. This contamination necessitates an urgent improvement in water treatment techniques [9]. Among these water treatment methods, Advanced Oxidation Processes (AOPs) remain highly promising for the oxidation of organic pollutants. AOPs are based on the in situ production of highly oxidizing and reactive radical species that interact with organic pollutants and lead to their fragmentation. The hydroxyl radical is a highly reactive and relatively non-selective species that exhibits a strong oxidizing character [10-12]. Heterogeneous photo-catalysis involves naturally or artificially irradiating an intrinsic or extrinsic semiconductor material, such as TiO_2 or ZnO, also known as a photo-catalyst [13-14]. The semiconductor is photo-excited by photons with energy equal to or greater than the bandgap energy (EC-EV). An electron is liberated within the semiconductor and undergoes an energy transition from the Valence Band (VB) to the Conduction Band (CB). During this transition, electron vacancies, commonly referred to as "holes" (h+), and an excess of electrons (e-) are created within the material. The use of nanoparticles as photo-catalysts is a highly beneficial approach to harness the physical and optical properties of semiconductors, as described in [14-16]. NPs incorporated into a photo-catalyst are extremely tiny particles, typically in the nanometer scale. These NPs play a crucial role in enlarging the photo-catalytic activity. The reduced size of these nanoparticles results in a significant increase in the surface area-to-volume ratio, providing more active sites for photo-catalytic reactions [17, 18]. This enlarged surface area also enhances light absorption, leading to improved photo-catalytic efficiency. Moreover, the small size of NPs facilitates the diffusion of reactants and products, thereby enhancing the overall reaction kinetics. By precisely controlling the size, shape, and composition of the NPs, the photo-catalytic performance of the material for specific applications can be optimized [19, 20].

Authors in [21] investigated the degradation of sulfamethoxazole (SMX) using a synthesized ZnO-NPs catalyst and UVA irradiation. ZnO-NPs were synthesized through a simple hydrothermal-assisted method. The research examined the influence of various factors, including ZnO heating time and synthesis reaction, pH, catalyst loading, and initial SMX concentration, on the efficiency of the degradation process. Morphological changes in the ZnO were observed after the photo-catalytic treatment. The study confirmed that SMX degradation occurred through the action of hydroxyl radicals. In the same context, authors in [22] showed that the photo-catalytic performance of SMX degradation is enhanced with cobalt doping, and the hetero-structure doped with 3% Co demonstrates the highest degradation efficiency. Authors in [23] indicate that an acidic medium is more favorable for the degradation of SMX, with the optimum pH values for UV/TiO_2 and UV/WO_3 being 4 and 3, respectively. The determined optimal dosage of TiO_2 and WO_3 was 500 mg/L and 750 mg/L, resulting in removal efficiencies of 61.28% and 43.3%, respectively. Despite the significant number of research studies on the application of photo-catalysis for the degradation of SMX, only a few studies have focused on the effect of reducing the size of ZnO-NPs on the degradation of this pollutant. It is within this context that this work aims to contribute to the characterization of ZnO-NPS and the study of the impact of experimental synthesis conditions of nanoparticles on the improvement of photo-catalytic degradation. In addition, a numerical modeling of coupled transport and reaction phenomena will be presented.

II. EXPERIMENTAL

A. Organic Pollutant

The pollutant chosen is Sulfamethoxazole (SMX). A Thermo Scientific Evolution_300 spectrophotometer was used to identify SMX from its absorption spectrum. The spectral range of the spectrometer is from 190 to 1100 nm. The precision is ± 1 nm, the reproducibility is 0.1 nm, and the scanning speed is 240 nm/min. The residual concentrations were obtained by interpolation using the calibration curves or spectra A = f(λ). SMX absorbs in the UV-Visible at the wavelength of 258 nm as shown in Figure 1.

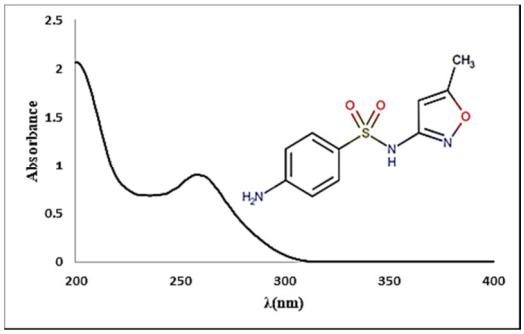

Fig. 1. UV-visible absorption spectrum of SMX.

B. ZnO Synthesis Protocol

The sol-gel method was utilized to synthesize ZnO nanoparticles. Zinc acetate (Z.A) and sodium hydroxide

(NaOH) were used as precursors, and the mixture in mol/L ([Zn]/[NaOH]=0.5/0.5) was prepared in a solvent composed of distilled water and ethanol. In order to achieve homogeneous solution, both solutions, the Z.A solution (A) and the NaOH solution (B) were thoroughly mixed with the solvent while stirring at a speed of 600 rpm for a period of 15 min. Then, 160 ml of solution (B) were gradually added to 80 ml of solution (A) with magnetic stirring (600 rpm) in a water bath at a specific temperature (°C) under reflux conditions. At the end of this step, a white gel was formed. The obtained product underwent centrifugation at 3000 rpm for 5 min, followed by filtration and thorough rinsing with acetone solution and distilled water to eliminate any residues. Finally, the product was dried in an oven at 80°C for 24 hr and then calcined at 500°C for 4 hr to remove any remaining organic chains, water vapors, and trapped solvents. The experimental protocol flowchart is shown in Figure 2.

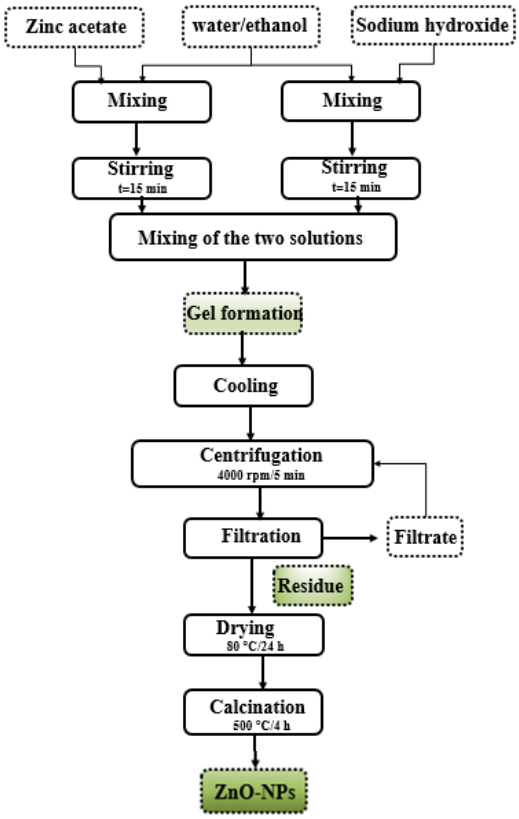

Fig. 2. ZnO-NP synthesis flow chart using the sol-gel method.

C. Characterization of ZnO-NPs

The produced ZnO-NPs were examined for structure and crystallinity with the XRD method. Analysis was carried out using a D8 Advance Bruker diffractometer with Cu-K radiation (= 0.15406 nm) and an accelerating voltage ranging from 20 to 80°C at roughly 40 kV. The width of the diffraction peak varies with the size of the crystallites in the sample. The broadening of the diffraction peak occurs for very small crystals. The measurement of the Full Width at Half Maximum (FWHM) of the most intense peaks allows to estimate the average grain size "D" using the Debye-Scherrer equation [24]:

$$D = \frac{K\lambda}{\beta \cos\theta} \quad (1)$$

D. Photocatalytic Tests

The photocatalytic activity of SMX was evaluated using a microstructured polymer reactor with 150 mm length, 2 mm width, and 1 mm depth. A solution containing synthesized ZnO-NPs at a concentration of 100 mg/L was deposited in the microchannel. A quantity of 10 mg/L of the stock solution was introduced into the microchannel via a syringe pump. The photocatalytic test consisted of two stages. In the first stage, the SMX solution was circulated through the microchannel in the absence of light to allow the adsorption of SMX onto the surface of the photocatalyst. The second stage involved the irradiation of the photocatalyst (I=1.5 mW/cm^2) in the presence of dissolved oxygen to ensure the photocatalytic degradation process. Figure 3 illustrates the experimental device for the photo-catalytic tests.

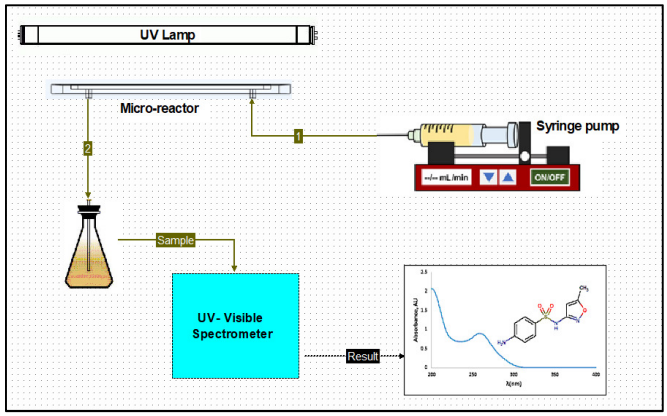

Fig. 3. Experimental device for the photo-catalytic tests.

The concentration of SMX was measured at the outlet of the reactor every 5 min using a Thermo Scientific Evolution 300 UV-Visible spectrophotometer. The mesurment steps include sample preparation, spectrophotometer calibration, and absorbance measurement at the specific wavelength of 257 nm, concentration calculation via the Beer-Lambert Law, and subsequent validation and interpretation of the measured concentration. Finally, the degradation efficiency (DE) of the nanoparticles was estimated by:

$$\mathrm{DE} = \left(1 - \frac{C_o}{C_i}\right) * 100\% \quad (2)$$

where C_i and C_o represent the concentrations at the inlet and outlet of the microchannel, respectively.

E. Modeling and Simulation

The degradation of SMX through photo-catalysis proceeds through several stages that involve coupled processes, such as the transportation of molecules and chemical reactions [25, 26]. To solve the mathematical equations governing the transport and photocatalytic reaction, COMSOL Multiphysics simulation software was utilized. This software enables the integration of

flow phenomena, pollutant transport via convection and diffusion, and chemical reactions. The equations for conserving mass and momentum were obtained by global and partial balances within the microreactors. The following assumptions were considered: Gravity forces have no effect on the flow within the microreactors, the flow regime is characterized as laminar, and the fluid is both Newtonian and incompressible. Consequently, the photocatalytic degradation of SMX can be formulated as follows [26]:

$$\frac{\partial C}{\partial t} + \nabla . J + u . \nabla c = \frac{kKC}{1+KC} \quad (3)$$

where c represents the concentration of SMX (sulfamethoxazole), J is the mass transfer flux of SMX towards the catalytic surface, u refers to the flow velocity of the solution containing the pollutant, k represents the kinetic rate constant of the reaction, and K gives the adsorption constant of SMX onto the photocatalyst surface.

III. RESULTS AND DISCUSSION

A. Characterization Results

The X-ray diffractometer displays various peaks that correspond to the crystal lattices of the material. The positions and intensities of these peaks can be used to identify the crystalline structure, and estimate particle size. The diffraction diagram for ZnO-NPs is shown in Figure 4.

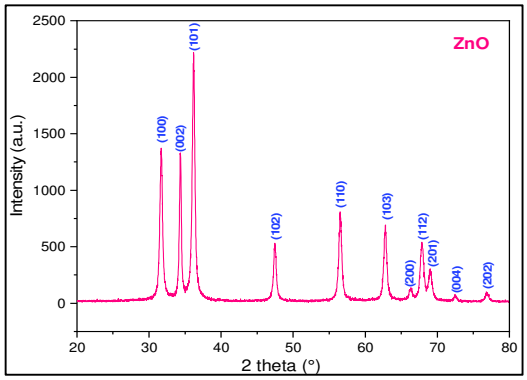

Fig. 4. X-ray diffraction diagram of ZnO NPs synthesized by sol-gel CAZ/CNaOH = 0.5/0.5, T = 60°C, tm=3 hr.

All characteristic peaks of ZnO are located within the range of 20° < 2θ < 80°, further confirming the presence of the metal oxide (ZnO). The high intensity and narrow peak width indicate the good crystallinity of the ZnO NPs. There are no additional peaks in the XRD patterns, indicating the high purity of the synthesized ZnO NPs. The determination of NP size was estimated by XRD using (1), allowing studying the influence of temperature and stirring time on the NP formation process, as shown in Figure 5. Figure 5 illustrates the variation in NP size obtained by the Scherrer method as a function of temperature. The average size of the NPs slightly decreases, initially, for both temperatures (50 and 60°C), but for the other temperatures, the decrease is approximately 4 nm. The grain growth is faster at higher temperatures (70, 80, and 90°C) after 3.5 hr, while at lower temperatures (50 and 60°C), this occurs after 4 hr. This phenomenon can be explained by the significant impact of temperature on the nucleation and aggregation of ZnO NPs. In general, higher temperatures can accelerate the rate of formation and growth of NPs, while lower temperatures can slow down these rates. However, the specific effects of temperature on the formation and aggregation can vary depending on different factors such as reaction conditions, NP morphology, precursor concentration, and solvent properties.

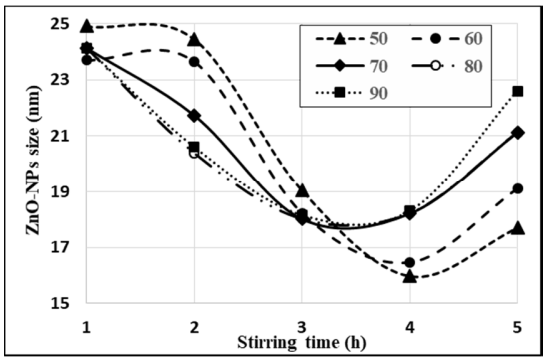

Fig. 5. Influence of temperature and stirring time on NPs.

Additionally, at higher temperatures, the reaction rate of precursor molecules may increase, leading to faster formation and growth of ZnO NPs. This can promote the formation of larger NPs and increase the probability of aggregation, where particles stick together to form larger clusters. On the other hand, at lower temperatures, the reaction rate may decrease, resulting in slower formation and growth of NPs. This can lead to the formation of smaller NPs and reduce the probability of aggregation [27, 28]. The best result obtained (the smallest NP size of ZnO) corresponds to a temperature of T = 50°C and a mixing duration of 4 hr.

B. Photo-Catalytic Test Results

The photo-catalytic degradation experiments were performed using two different photo-catalysts of ZnO-NPs: one commercially available and the other synthesized through the sol-gel method. The particle sizes of these photo-catalysts were 50 nm and 16 nm, respectively. Figure 6 combines the results of SMX adsorption on the photo-catalyst, SMX photolysis, and photo-catalytic degradation.

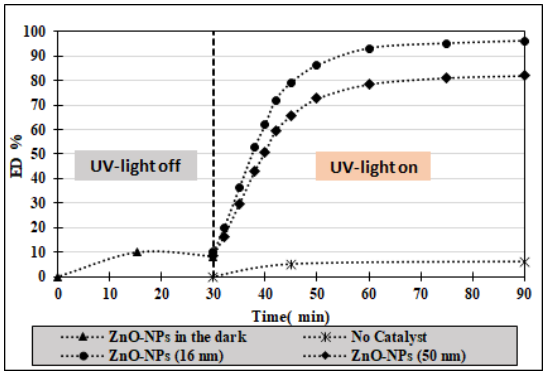

Fig. 6. SMX adsorption, photolysis, and photo-catalytic degradation.

Figure 6 shows that in the absence of UV irradiation (between 0 and 30 min), SMX molecules adsorb onto the ZnO-NPS photo-catalyst and the conversion rate reaches 10% at 15 min. Subsequently, there is a slight decrease in the conversion rate (DE=8%), reaching adsorption –desorption equilibrium at 30 min. On the other hand, in the presence of irradiation, two phenomena can be distinguished. In the absence of a photo-catalyst, the photolysis phenomenon causes a slight degradation of SMX on the order of 6%. In the presence of UV irradiation and a photo-catalyst, the photo-catalytic degradation is more pronounced on the ZnO –NPs with a size of 16 nm. With this size, the conversion rate reaches 96%, while commercial ZnO-NPs only degrade 81% of SMX. Reducing the size of NPs enhances the efficiency of photo-catalytic degradation for several reasons. Firstly, smaller ZnO-NPs have a larger surface area per unit mass, providing more active sites for pollutant adsorption and reaction. Additionally, their smaller size allows more efficient light absorption, as they exhibit higher light absorption efficiency due to the quantum confinement effects. This leads to increased generation of electron-hole pairs, which are crucial for the photo-catalytic process. Moreover, the shorter diffusion paths in smaller NPs facilitate faster mass transport and reaction kinetics, the higher surface-to-volume ratio of smaller NPs reduces electron-hole recombination, as more surface sites are available for charge separation [29-31]. In summary, reducing the size of ZnO NPs optimizes surface area, light absorption, diffusion, and charge separation, ultimately improving the efficiency of the photo-catalytic degradation.

C. Modeling and Simulation

COMSOL Multiphysics simulation software was employed to solve the mathematical equations governing the transport and photo-catalytic reaction involved in the degradation of SMX. This process occurs in multiple stages and involves coupled processes, including molecule transportation and chemical reactions. The geometry of the micro-reactor is presented in Figure 7.

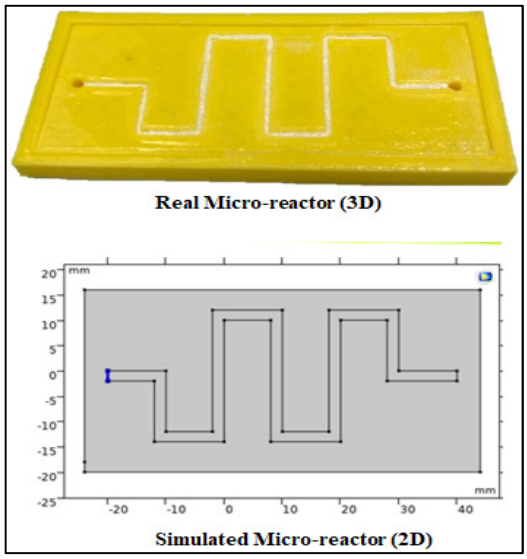

Fig. 7. Geometry of the micro-reactor.

The decision to conduct the micro-reactor simulation in 2D is based on the objective of reducing computational time while still capturing the essential physical aspects of the system. By simulating the micro-reactor in two dimensions instead of three, the complexity of the calculations is significantly reduced, leading to faster simulation times. A study of the meshing reveals that the physical results, such as flow velocity, remain unchanged when the mesh size was below 10 µm as shown in Figure 8. It is observed that the mesh is finer near the boundary zones (micro-reactor walls) where the flow velocity is assumed to be zero.

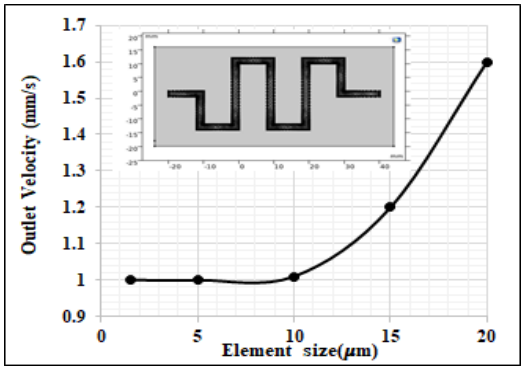

Fig. 8. Meshing of the micro-reactor geometry.

The numerical solving of (2) enabled the plotting of velocity and concentration profiles within the micro-channel containing the photo-catalyst as shown in Figure 9.

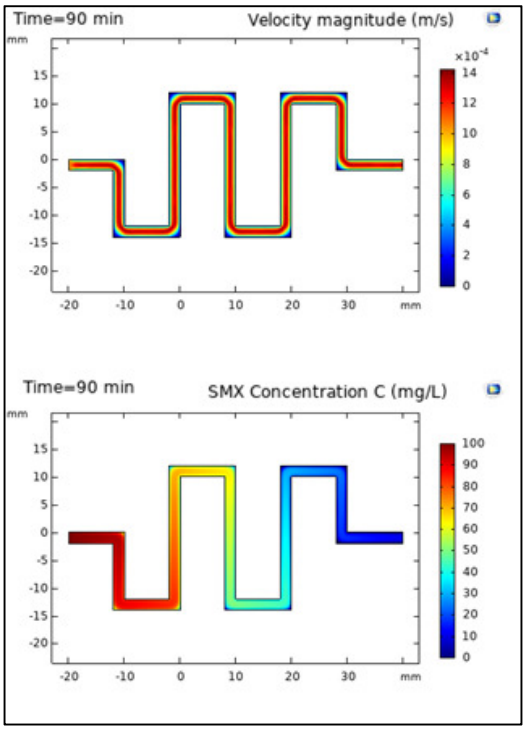

Fig. 9. Velocity and concentration profiles within the micro-channel.

The flow velocity profile in the micro-channel shows a homogeneous distribution, with maximum velocity at the center and zero velocity near the walls. It is important to mention that the fluid undergoes rapid changes in direction when passing through the bends, leading to localized stagnant zones within the velocity profile. On the other hand, the concentration of SMX decreases along the entire micro-channel, reaching a value of 2.5 mg/L at the outlet, corresponding to a conversion rate of 97.5%. It is interesting to note that in stagnant fluid zones, the concentration of SMX is zero. This can be explained by the prolonged residence time of SMX molecules on the photo-catalyst surface, leading to their complete degradation.

The simulation of photo-catalytic degradation allowed for a comparative analysis between the experimental results and the simulation data. Two distinct simulations were performed as shown in Figure 10. The first focused on the adsorption of SMX from the photo-catalyst surface, utilizing the Langmuir-Hinshelwood model. The kinetic and adsorption constants used in the simulation were experimentally determined. The second simulation involved the photo-catalytic degradation process, considering an apparent kinetic constant that varied with the light intensity ($k_{app} = k_0 \times I$). By conducting these simulations, a comprehensive understanding of the photo-catalytic degradation process was obtained, facilitating the comparison between the experimental and the simulated results.

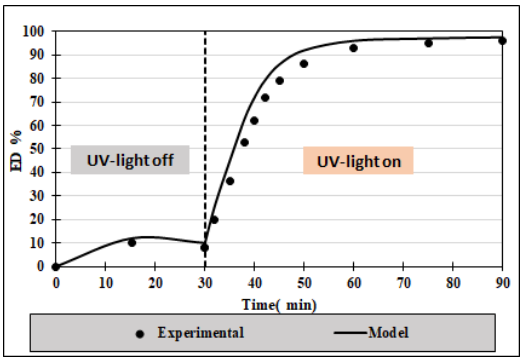

Fig. 10. Comparison between the experimental and the simulated results.

Figure 10 illustrates that the conversion rate obtained through simulation is slightly higher than that achieved during the experiments. This difference, which amounts to approximately 2%, can be attributed to the perfectly homogeneous dispersion of the photo-catalyst in the simulation, whereas in the experimental setup, there may be some variations in the dispersion. However, this difference remains negligible, and overall, the model fits well with the experimental data. This validation of the chosen model confirms its reliability and accuracy.

IV. CONCLUSION

A successful synthesis of ZnO-NPs was carried out under different time and mixing conditions. The XRD characterization revealed good crystallinity of the produced NPs and high purity. Particle size determination under various conditions showed a slight decrease in the average size of the NPs at 50°C and 60°C. However, for the other temperatures, the decrease is approximately 4 nm. The grain growth is faster (3.5 hr) at higher temperatures (70, 80, and 90°C), and slower (4 hr) at lower temperatures (50 and 60°C). This can be explained by the significant impact of temperature on the nucleation and aggregation of ZnO NPs. The photo-catalytic degradation experiments were performed using two different photo-catalysts of ZnO-NPs. The photo-catalytic degradation is more efficient on the ZnO –NPs with a size of 16 nm. With this size, the conversion rate reaches 96%, while commercial ZnO-NPs only degrade 81% of SMX. Smaller ZnO-NPs have a larger surface area per unit mass, providing more active sites for pollutant adsorption and reaction. Additionally, their smaller size allows more efficient light absorption, as they exhibit higher light absorption efficiencies due to the quantum confinement effects. The coupled model simulating the transport and photo-catalytic degradation of SMX fits well with the experimental data. This validation of the chosen model confirms its reliability and accuracy.

ACKNOWLEDGMENTS

The authors gratefully acknowledge the approval and support of this research study by the grant no. ENGA-2022-11-1833 from the Deanship of Scientific Research at Northern Border University, Arar, Kingdom of Saudi Arabia.

REFERENCES

[1] N. Akhtar, M. I. Syakir Ishak, S. A. Bhawani, and K. Umar, "Various Natural and Anthropogenic Factors Responsible for Water Quality Degradation: A Review," *Water*, vol. 13, no. 19, Jan. 2021, Art. no. 2660, https://doi.org/10.3390/w13192660.

[2] M. V. Japitana and M. E. C. Burce, "A Satellite-based Remote Sensing Technique for Surface Water Quality Estimation," *Engineering, Technology & Applied Science Research*, vol. 9, no. 2, pp. 3965–3970, Apr. 2019, https://doi.org/10.48084/etasr.2664.

[3] N. Morin-Crini *et al.*, "Worldwide cases of water pollution by emerging contaminants: a review," *Environmental Chemistry Letters*, vol. 20, no. 4, pp. 2311–2338, Aug. 2022, https://doi.org/10.1007/s10311-022-01447-4.

[4] Y. Chen, L. Song, Y. Liu, L. Yang, and D. Li, "A Review of the Artificial Neural Network Models for Water Quality Prediction," *Applied Sciences*, vol. 10, no. 17, Jan. 2020, Art. no. 5776, https://doi.org/10.3390/app10175776.

[5] A. Saravanan *et al.*, "Effective water/wastewater treatment methodologies for toxic pollutants removal: Processes and applications towards sustainable development," *Chemosphere*, vol. 280, Oct. 2021, Art. no. 130595, https://doi.org/10.1016/j.chemosphere.2021.130595.

[6] M. Godoy and J. Sanchez, "Antibiotics as Emerging Pollutants in Water and Its Treatment," in *Antibiotic Materials in Healthcare*, V. Kokkarachedu, V. Kanikireddy, and R. Sadiku, Eds. Cambridge, MA, United States: Academic Press, 2020, pp. 221–230.

[7] E. Mendez, M. A. Gonzalez-Fuentes, G. Rebollar-Perez, A. Mendez-Albores, and E. Torres, "Emerging pollutant treatments in wastewater: Cases of antibiotics and hormones," *Journal of Environmental Science and Health, Part A*, vol. 52, no. 3, pp. 235–253, Feb. 2017, https://doi.org/10.1080/10934529.2016.1253391.

[8] E. Y. Klein *et al.*, "Global increase and geographic convergence in antibiotic consumption between 2000 and 2015," *Proceedings of the National Academy of Sciences*, vol. 115, no. 15, pp. E3463–E3470, Apr. 2018, https://doi.org/10.1073/pnas.1717295115.

[9] Q. Yang *et al.*, "Antibiotics: An overview on the environmental occurrence, toxicity, degradation, and removal methods," *Bioengineered*,

vol. 12, no. 1, pp. 7376–7416, Jan. 2021, https://doi.org/10.1080/21655979.2021.1974657.

[10] A. Z. Al-Khazaal, F. Ahmad, and N. Ahmad, "Study on the Removal of Thiosulfate from Wastewater by Catalytic Oxidation," *Engineering, Technology & Applied Science Research*, vol. 9, no. 2, pp. 4053–4056, Apr. 2019, https://doi.org/10.48084/etasr.2553.

[11] Y. Deng and R. Zhao, "Advanced Oxidation Processes (AOPs) in Wastewater Treatment," *Current Pollution Reports*, vol. 1, no. 3, pp. 167–176, Sep. 2015, https://doi.org/10.1007/s40726-015-0015-z.

[12] J. A. Garrido-Cardenas, B. Esteban-Garcia, A. Aguera, J. A. Sanchez-Perez, and F. Manzano-Agugliaro, "Wastewater Treatment by Advanced Oxidation Process and Their Worldwide Research Trends," *International Journal of Environmental Research and Public Health*, vol. 17, no. 1, Jan. 2020, Art. no. 170, https://doi.org/10.3390/ijerph17010170.

[13] H. Wang *et al.*, "A review on heterogeneous photocatalysis for environmental remediation: From semiconductors to modification strategies," *Chinese Journal of Catalysis*, vol. 43, no. 2, pp. 178–214, Feb. 2022, https://doi.org/10.1016/S1872-2067(21)63910-4.

[14] S. Gisbertz and B. Pieber, "Heterogeneous Photocatalysis in Organic Synthesis," *ChemPhotoChem*, vol. 4, no. 7, pp. 456–475, 2020, https://doi.org/10.1002/cptc.202000014.

[15] M. M. Nadareishvili, G. Mamniashvili, D. Jishiashvili, G. Abramishvili, C. Ramana, and J. Ramsden, "Investigation of the Visible Light-Sensitive ZnO Photocatalytic Thin Films," *Engineering, Technology & Applied Science Research*, vol. 10, no. 2, pp. 5524–5527, Apr. 2020, https://doi.org/10.48084/etasr.3392.

[16] O. Herrfurth, E. Kruger, S. Blaurock, H. Krautscheid, and M. Grundmann, "Hot-phonon effects in photo-excited wide-bandgap semiconductors," *Journal of Physics: Condensed Matter*, vol. 33, no. 20, Dec. 2021, Art. no. 205701, https://doi.org/10.1088/1361-648X/abf19b.

[17] H. S. Jarusheh, A. Yusuf, F. Banat, M. A. Haija, and G. Palmisano, "Integrated photocatalytic technologies in water treatment using ferrites nanoparticles," *Journal of Environmental Chemical Engineering*, vol. 10, no. 5, Oct. 2022, Art. no. 108204, https://doi.org/10.1016/j.jece.2022.108204.

[18] A. Bassi and I. Hasan, "A review on nanoparticles as photo catalyst for the treatment of wastewater," *AIP Conference Proceedings*, vol. 2735, no. 1, Sep. 2023, Art. no. 030001, https://doi.org/10.1063/5.0140499.

[19] K. Khan *et al.*, "Recent Progress, Challenges, and Prospects in Two-Dimensional Photo-Catalyst Materials and Environmental Remediation," *Nano-Micro Letters*, vol. 12, no. 1, Aug. 2020, Art. no. 167, https://doi.org/10.1007/s40820-020-00504-3.

[20] A. Das and M. K. Adak, "Photo-catalyst for wastewater treatment: A review of modified Fenton, and their reaction kinetics," *Applied Surface Science Advances*, vol. 11, Oct. 2022, Art. no. 100282, https://doi.org/10.1016/j.apsadv.2022.100282.

[21] T. Makropoulou, I. Kortidis, K. Davididou, D. E. Motaung, and E. Chatzisymeon, "Photocatalytic facile ZnO nanostructures for the elimination of the antibiotic sulfamethoxazole in water," *Journal of Water Process Engineering*, vol. 36, Aug. 2020, Art. no. 101299, https://doi.org/10.1016/j.jwpe.2020.101299.

[22] O. Mertah, A. Gomez-Aviles, A. Slassi, A. Kherbeche, C. Belver, and J. Bedia, "Photocatalytic degradation of sulfamethoxazole with Co-CuS@TiO2 heterostructures under solar light irradiation," *Catalysis Communications*, vol. 175, Feb. 2023, Art. no. 106611, https://doi.org/10.1016/j.catcom.2023.106611.

[23] F. Beheshti, R. M. A. Tehrani, and A. Khadir, "Sulfamethoxazole removal by photocatalytic degradation utilizing TiO2 and WO3 nanoparticles as catalysts: analysis of various operational parameters," *International Journal of Environmental Science and Technology*, vol. 16, no. 12, pp. 7987–7996, Dec. 2019, https://doi.org/10.1007/s13762-019-02212-x.

[24] S. Mustapha *et al.*, "Comparative study of crystallite size using Williamson-Hall and Debye-Scherrer plots for ZnO nanoparticles," *Advances in Natural Sciences: Nanoscience and Nanotechnology*, vol. 10, no. 4, Aug. 2019, Art. no. 045013, https://doi.org/10.1088/2043-6254/ab52f7.

[25] A. Asadi, A. Larimi, and A. Naderifar, "Modeling and simulation of photoreactor for photocatalytic conversion of CO 2 into methanol," in *11 th International Chemical Engineering Congress & Exhibition*, Fouman, Iran, Apr. 2020, pp. 1–6.

[26] A. Yusuf *et al.*, "Modelling of a recirculating photocatalytic microreactor implementing mesoporous N-TiO2 modified with graphene," *Chemical Engineering Journal*, vol. 391, Jul. 2020, Art. no. 123574, https://doi.org/10.1016/j.cej.2019.123574.

[27] M. Bandeira, M. Giovanela, M. Roesch-Ely, D. M. Devine, and J. da Silva Crespo, "Green synthesis of zinc oxide nanoparticles: A review of the synthesis methodology and mechanism of formation," *Sustainable Chemistry and Pharmacy*, vol. 15, Mar. 2020, Art. no. 100223, https://doi.org/10.1016/j.scp.2020.100223.

[28] E. Moyen, J. H. Kim, J. Kim, and J. Jang, "ZnO Nanoparticles for Quantum-Dot-Based Light-Emitting Diodes," *ACS Applied Nano Materials*, vol. 3, no. 6, pp. 5203–5211, Jun. 2020, https://doi.org/10.1021/acsanm.0c00639.

[29] T. Ahmed and T. Edvinsson, "Optical Quantum Confinement in Ultrasmall ZnO and the Effect of Size on Their Photocatalytic Activity," *The Journal of Physical Chemistry C*, vol. 124, no. 11, pp. 6395–6404, Mar. 2020, https://doi.org/10.1021/acs.jpcc.9b11229.

[30] M. R. Islam, M. Rahman, S. F. U. Farhad, and J. Podder, "Structural, optical and photocatalysis properties of sol–gel deposited Al-doped ZnO thin films," *Surfaces and Interfaces*, vol. 16, pp. 120–126, Sep. 2019, https://doi.org/10.1016/j.surfin.2019.05.007.

[31] F. M. Sanakousar, C. C. Vidyasagar, V. M. Jimenez-Perez, and K. Prakash, "Recent progress on visible-light-driven metal and non-metal doped ZnO nanostructures for photocatalytic degradation of organic pollutants," *Materials Science in Semiconductor Processing*, vol. 140, Mar. 2022, Art. no. 106390, https://doi.org/10.1016/j.mssp.2021.106390.